Earth and Planetary Science Letters 296 (2010) 373–383

Contents lists available at ScienceDirect

Earth and Planetary Science Letters

journal homepage: www.elsevier.com/locate/epsl

Using tracer thermochronology to measure modern relief change in the Sierra Nevada, California

Devin McPhillips *, Mark T. Brandon

Yale University, USA

ARTICLE INFO

Article history:
Received 11 December 2009
Received in revised form 14 May 2010
Accepted 18 May 2010
Available online 18 June 2010

Editor: T.M. Harrison

Keywords:
relief
thermochronology
isochrones
Sierra Nevada
gravitational instability

ABSTRACT

We examine relief change in two major Sierra Nevada drainages, the Kings and the San Joaquin. The modern distribution of bedrock cooling ages is derived by fitting isochrones to a dense distribution of existing cooling ages. This analysis indicates southwest tilting of the range by $3.4° \pm 0.8°$, which is consistent with other geologic evidence for tilting after ~5 Ma. The detrital cooling ages from the Kings show an excess of young ages relative to what would be expected from uniform erosion, whereas the San Joaquin drainage shows excess old ages. These results indicate increasing relief in the Kings. The results in the San Joaquin are more difficult to interpret due to the dense network of dams, which trap sediment. However, we analyze the effect of storage behind the dams and suggest steady or declining relief in the San Joaquin. The residence time of sediment in these drainages indicates that these relief estimates are averaged over the last 100 to 10 ka. We suggest that relief change is related to localized surface uplift in the southern Sierra Nevada, including the Kings drainage, caused by ongoing lower lithosphere removal. The San Joaquin drainage may be north of the lithospheric anomaly, which is consistent with stagnating or decaying relief there.

1. Introduction

The topography of a mountain range is best considered in terms of its two fundamental components, mean elevation and relief (e.g., Braun, 2003). Relief, which is defined as the variation of topography around an arbitrary mean surface, is often the most striking feature of a mountain range. At the surface, relief is the result of competing geomorphic processes including river incision, mass wasting, and chemical weathering. Molnar and England (1990) emphasized the influence of relief on the isostatic response of the lithosphere. At depth, relief has significant control on the thermal structure of the crust and thereby on the closure depth of thermochronometers. Braun (2002) has taken advantage of this control to measure relief change over long timescales. Though important, changes in relief are difficult to measure. For example, river incision provides some insight into relief change, but complimentary measurements of the change in height of interfluves are needed for a full estimate of relief change. Here we introduce a new method for measuring relief change by tracer thermochronology and demonstrate it in two adjacent drainages in the Sierra Nevada, California.

Most commonly, thermochronology is used to measure mean erosion rates and to understand erosion and exhumation at large temporal and spatial scales. We focus exclusively on erosion here given that the eroded compliment to the Sierra Nevada is present in sedimentary sequences to the west (Linn et al., 1992). The lowest-temperature thermochronometer in wide use is apatite (U–Th)/He, which has a closure temperature of ~70 °C, corresponding to a depth of ~3 km in continental crust (e.g., Reiners and Brandon, 2006). Conventional thermochronology can be used to estimate time-averaged erosion rates of bedrock, as represented by the time-of-flight from the closure surface to the topographic surface. We call this a TF (time-of-flight) method. The age-elevation (AE) method measures the rate that rocks move through the closure surface. The AE method provides an estimate of the erosion rate at the time of the cooling age, whereas the TF method provides an estimate of the average erosion rate from the cooling age to present. These estimates are averaged over long time scales, and thus tend to represent regional-scale erosion rates given that geomorphic processes tend to migrate spatially on shorter time scales.

Detrital dating of the minerals in the sediment load in river drainages provides an alternative for examining erosion processes. The lag-time method (Garver and Brandon, 1994; Bernet et al., 2009) has been used to estimate long-term erosion rates at the scale of an entire orogen. Cosmogenic nuclides in detrital sediment provide a mean erosion rate at shorter timescales in local drainages (e.g., Bierman and Nichols, 2004). In fact, as emphasized by Bernet et al. (2009), cosmogenic and thermochronologic detrital methods are essentially identical in design because both depend on measuring the time-of-flight through a zone of radiogenic accumulation. Variants of these methods have been exploited in interesting ways by Stock and

* Corresponding author. Yale University, P.O Box 208109 New Haven, CT 06520, USA. Tel.: +1 510 847 9607; fax: +1 203 432 3134.
E-mail addresses: devin.mcphillips@yale.edu (D. McPhillips), mark.brandon@yale.edu (M.T. Brandon).

0012-821X/$ – see front matter © 2010 Elsevier B.V. All rights reserved.
doi:10.1016/j.epsl.2010.05.022

Montgomery (1996), Brewer et al. (2003), Stock et al. (2006), Vermeesch (2007), and Gayer et al. (2008), among others.

Our approach uses detrital cooling ages as a tracer, which links modern stream sediment to upstream bedrock sources. For example, Vermeesch (2007) used cooling ages to constrain the source of alluvial boulders to upstream bedrock sources. At the drainage-scale, Stock et al. (2006) used a tracer method to argue for above-average erosion rates in the upper reaches of a drainage because of the abundance of old cooling ages in the fluvial sediment. In this study, we establish a statistical basis for the tracer thermochronology method and demonstrate the method's promise using two natural examples.

We present our erosion rate calculations in three steps. First, we estimate bedrock ages over the surface of the catchment (Fig. 1A). Brewer et al. (2003) and Ruhl and Hodges (2005) have used the AE method to estimate the surface distribution of bedrock cooling ages, but this approach carries the assumption that isochrones, defined as surfaces of equal cooling age, are everywhere horizontal. Our approach explicitly estimates the geometry of the isochrones (Fig. 1C–D). Second, we discuss the detrital sampling method and its underlying assumptions including the influence of sediment storage, either by natural process or by man-made dams (Fig. 1A). Third, we borrow from the literature of probability density estimation and outline a method for estimating densities and relative erosion rates (Fig. 1B). The resulting erosion rate distributions can be mapped back onto the topographic surface. The spatial variation of erosion provides direct information on relief change on the time scale of 100 to 10 ka.

Our application of the tracer method focuses on the Kings and San Joaquin rivers, which are large adjacent drainages (>3000 km^2) located on the western slope of the Sierra Nevada (Fig. 2). The evolution of relief in this area is much debated (e.g., House et al., 1997; Wakabayashi and Sawyer, 2001; Clark et al., 2005). The presence of numerous dams above the detrital sampling point in the San Joaquin also provides an opportunity to examine how unsteady storage might influence our method. Widespread (U–Th)/He apatite ages, available from the literature, are adequate to estimate the bedrock distribution of cooling ages. We present detrital (U–Th)/He apatite ages that were collected from stream sediment the foothills of the drainages. We begin by introducing the geologic setting of the Sierra Nevada and then develop the tracer method in parallel with the application in order to provide a clear, step-by-step demonstration.

2. Setting

The Sierra Nevada is largely underlain by Mesozoic granitic batholiths. In the north, Tertiary volcanic and sedimentary rocks overlie the batholiths. These younger strata record a few degrees of westward tilt since ~5 Ma (e.g., Unruh, 1991). Tilting was roughly coincident with ~0.5 km incision by major rivers, including the San Joaquin (Wakabayashi and Sawyer, 2001). To the south, direct evidence of tilting is scarce because Tertiary cover is absent, but the modern average slope of the west flank of the Sierra in our study area is almost 2°. The southern Sierra Nevada is more faulted than in the north (Dixon et al., 2000; Maheo et al., 2009), so there may also be local tilting of smaller, fault-bounded blocks. Recent evidence from relict landscapes of the southernmost Sierra supports westward tilting as well (Saleeby et al., 2009). River gorges in the south, including the Kings

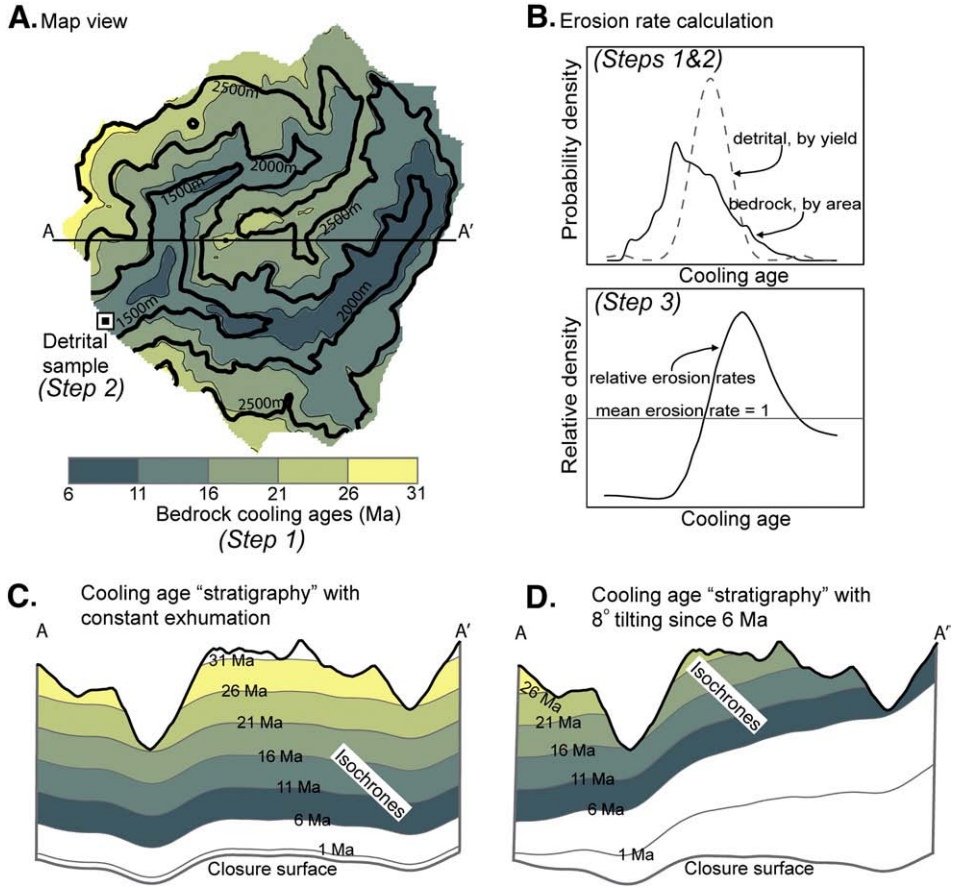

Fig. 1. Schematics illustrating the method for calculating relative erosion rates and the effects of isochrone deformation on surface bedrock ages. A) In the map view, topographic contours are heavy black lines, bedrock cooling ages are shaded and cut across contours, and the squares signify the location of detrital sampling. B) Density plots show how relative erosion rates are calculated as a relative density from bedrock- and detrital-age distributions. C) Hypothetical cross section illustrating the relatively flat isochrones produced at the closure surface by constant exhumation rates and constant topography. D) Cross section of map view in part (A), illustrating the isochrone structure at depth resulting from constant exhumation followed by 8° of tilting since 6 Ma.

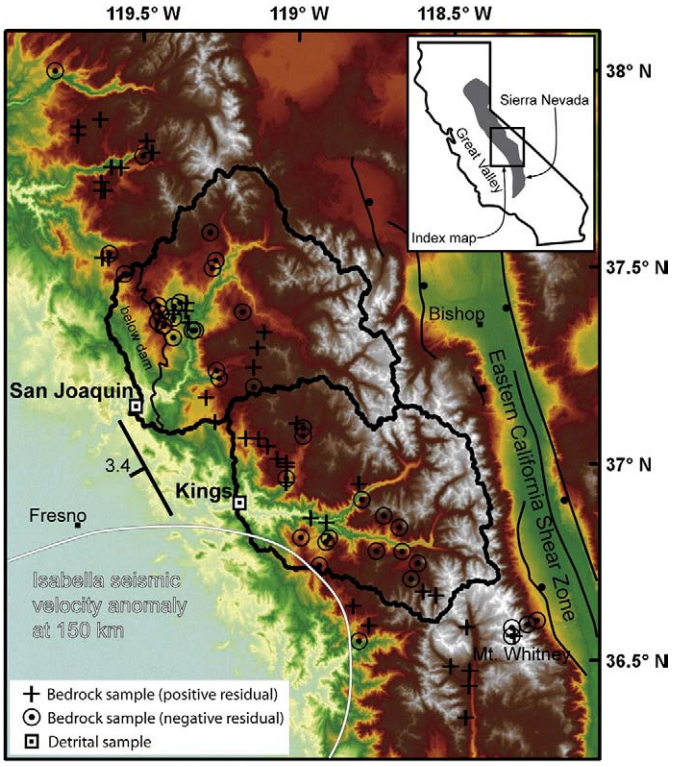

Fig. 2. Topographic map of the study area in the central and southern Sierra Nevada. The San Joaquin and Kings River drainages are outlined in heavy black lines. In the San Joaquin, the smaller drainage area between the detrital sampling point and the first trunk stream dam is also outlined. Sampling locations for bedrock and detrital cooling ages are shown. Bedrock samples are shown as crosses and bulls-eyes, where crosses indicate a positive residual in the best-fit isochrone model and bulls-eyes indicate negative residuals. The strike and dip symbol shows the orientation of the best-fit isochrone surfaces. The location of the Isabella seismic velocity anomaly at 150 km depth is shown (Ruppert et al., 1998). Normal faults associated with the Eastern California Shear Zone are shown in Owen's Valley.

River, were incised ~0.5 km between 5 to 3 Ma (Stock et al., 2004; Stock et al., 2005). The cause of this pulse of incision remains uncertain and possibilities include a flexural response to Basin and Range extension (e.g., Chase and Wallace, 1988), the loss of a dense lithospheric root (e.g., Ducea and Saleeby, 1996; Farmer et al., 2002), and erosional unloading (Small and Anderson, 1995).

At present, drainage-scale relief of the Sierra Nevada generally increases along strike, from <1 km in the north to >2 km in the south. Mean elevations and summit elevations also show the same increase from north to south. Higher elevations everywhere are glacially sculpted, but there is also dramatic relief below the equilibrium line altitude of the Last Glacial Maximum (LGM), where sloping low-relief surfaces are cut by deep river gorges (Wahrhaftig and Birman, 1965; Clark et al., 2005). The San Joaquin and Kings Rivers occupy the transition between the northern and southern topographic styles of the range. This transitional area includes the majority of peaks over 4.0 km and many of the deepest gorges (Fig. 2).

Our tracer method measures relative erosion rates averaged over the time scale of sediment transport from bedrock source to the detrital sample location. This transport time is equivalent to the average residence time of unconsolidated sediment in the drainage, which we estimate as equal to the total volume of mobile sediment in the drainage divided by the average flux of that sediment through the drainage. By estimating these values from all available sources, we derive order-of-magnitude estimates of 100 to 10 ka for both drainages (see Supplementary materials).

Natural and man-made dams may degrade the utility of our tracer method. The Kings River is still largely a wild river, with dams impounding only 15% of the drainage area upstream of our sample site. In contrast, dams on the San Joaquin River enclose 90% of the drainage area upstream of our sample site. Janda (1966) estimated the sediment yield of the San Joaquin River has remained relatively fairly steady despite the presence of the dams. An explanation is that sediment captured behind the dams is replaced by erosion of bedrock and fill along the downstream channel. Our initial analysis below ignores the dams as a start. We follow with an assessment of how the dams on the San Joaquin might distort our results.

3. Defining probability distributions

In order to measure the spatial variation in erosion rates (and thereby relief change), we use probability distributions to quantify the relative contribution of all bedrock sources to the drainage sediment load. The fundamental data are thermochronometer ages from surface bedrock and sand-size detritus carried in the river. The bedrock grain ages are distributed by area over the topographic surface of the drainage, whereas the detrital grains are distributed by volume in the erosional yield. We define two random variables, T_A and T_V, to represent these age data, by area and volume respectively. The cumulative distribution functions (CDFs) for these variables are given in the usual way by

$$\begin{aligned} F_A(\tau) &= \Pr(T_A \leq \tau), \\ F_V(\tau) &= \Pr(T_V \leq \tau), \end{aligned} \tag{1}$$

where the function $\Pr(T \leq \tau)$ gives the probability that the random variable T takes on values less than or equal to a specified age τ, and F is the CDF. The probability density is defined as the derivative of the CDF:

$$\begin{aligned} f_A(\tau) &= \frac{dF_A(\tau)}{d\tau}, \\ f_V(\tau) &= \frac{dF_V(\tau)}{d\tau}. \end{aligned} \tag{2}$$

In practice, we can only estimate these distributions from discrete samples of bedrock and detrital ages, $T_{A,i}$ and $T_{V,j}$. The empirical cumulative probability distribution is a useful estimator that is defined as

$$\begin{aligned} \hat{F}_A(\tau) &= \frac{1}{m}\sum_{i=1}^{m} I\left(T_{A,i} \leq \tau\right), \\ \hat{F}_V(\tau) &= \frac{1}{n}\sum_{j=1}^{n} I\left(T_{V,j} \leq \tau\right), \end{aligned} \tag{3}$$

where $I(\bullet)$ is the indicator function, giving a value of one when true and zero when false.

4. Isochrones and surface bedrock ages

4.1. The isochrone perspective

A fundamental concept in thermochronology is that a mineral system closes, meaning that it starts to record time, at a specific, effective closure temperature (Dodson, 1973; also review by Reiners and Brandon, 2006). In reality, a thermochronometer closes over a temperature interval, but this interval can be represented by the effective closure temperature, which will vary as a function of erosion rate and thermal gradient. This isotherm can be viewed as a closure surface. In principal, we would expect that a thermochronometer would give the same age for all rocks located at the closure surface at the same time. In practice, we would expect some variation due to the precision and quality of the cooling ages.

One can envision that uplift of rocks through the closure surface produces a continuously varying field of cooling ages, which can be viewed as consisting of surfaces of constant age, which we call isochrones. This term is already used in stratigraphy to indicate surfaces of constant age (Bates and Jackson, 1987). We find it helpful in describing a concept that has long been implicit in the interpretation of thermochronologic data.

A single isochrone represents a smoothed version of the surface topography due to the downward continuation of the thermal field from the Earth's surface (Mancktelow and Grasemann, 1997). Isochrones are created, or "enisochronated", as continuous surfaces. In fact, in this sense, they represent an upside-down stratigraphy, which increases in age upward and away from the closure surface (Fig. 1A and C). Stratigraphic analysis of sedimentary sequences is likewise organized around the concept of isochrones. We contend that thermochronologic isochrones can be exploited in the same manner as stratigraphic isochrones to identify faults, folds, tilting, and other kinds of deformation.

These ideas of the thermochronological isochrone are generalized from the AE method of Wagner and Reimer (1972), who recognized that low-temperature cooling ages often show a strong, positive correlation with elevation. This correlation was interpreted to be the record of the upward motion of rocks through the closure isotherm. In essence, this AE method implicitly assumes that isochrones remain approximately flat, parallel to the closure isotherm where they were formed. In contrast, our concept of an isochrone accounts for the fact that rocks are commonly deformed after passing through the closure depth. We have discovered examples, not only in the Sierra Nevada, but also the Swiss Alps, where cooling ages do not correlate with elevation. Instead, the ages define a set of dipping isochronal planes. It is widely recognized that the closure isotherm is not flat, but in fact tends to be a highly smoothed, low-amplitude version of the surface topography (Braun, 2002). Thus, one might expect that isochrones might have an initial dip near the regional-scale dip of the overlying topography, which dips less than 2° in our study area.

In the Sierra Nevada, House et al. (2001) implicitly accounted for isochrone deformation by correcting their AE transects for 2° of tilting. Maheo et al. (2009) also implicitly recognized tilted isochrones in the southernmost Sierra Nevada, which they attributed to Cenozoic faulting. We provide a direct estimate of isochrone tilting. Our main focus here is to define the isochronal structure well enough so that we can make a map of the distribution of bedrock cooling ages in the Kings and San Joaquin drainages. Our best-fit model provides an estimate of the cooling, erosion, and tilt history of the southern Sierra Nevada, which are topics of interest in their own right (e.g. Wakabayashi and Sawyer, 2001).

4.2. Estimating bedrock-age distributions

Consider a set of samples, $i = 1$ to n, collected at locations indicated by E_i, N_i, and Z_i, which refer to the easting, northing, and vertical distances relative to an arbitrary origin. The samples are then dated, resulting in a set of ages τ_i in Ma. A dipping set of isochrones is defined by

$$\tau_i = b_E E_i + b_N N_i + b_Z Z_i + \tau_0, \quad (4)$$

where b_E, b_N, b_Z, and τ_0 are unknown parameters. The age gradient normal to these planes has units of Ma/km, which is the inverse of the average velocity of the dated rocks relative to the effective closure isotherm. In other words, this parameter provides a tilt-corrected AE erosion rate, assuming of course that the closure isotherm remains relatively stationary during closure.

We use a dataset of 88 published (U–Th)/He ages (Dumitru, 1990; House et al., 1997; House et al., 1998; House et al., 2001, Clarke et al., 2005) that span the San Joaquin and Kings drainages (Fig. 2). The model is fit to the data by finding values for the unknown parameters that minimize the L_1 norm, which is the sum of the absolute values of the difference between model predications and observed data. The conventional least-squares method (L_2 norm) provides similar estimates, but we prefer the L_1 norm because it is less sensitive to outliers (Menke, 1984). Fig. 3 shows the "reduced-age" projection of the data and model into a cross section oriented perpendicular to the best-fit strike of the isochrones. The line represents the predicted age at the elevation of the centroid of the data (2.2 km), and the observed ages have been reduced to this elevation using the gradients determined by the model fit. The offsets in age between the line and the data are directly equivalent to the residuals. One can see that there is a good fit between the model and the data ($R^2 = 0.68$), but the residuals are clearly larger than the error bars, which represent the estimated analytical uncertainties for the ages. This result is not unexpected given that the natural setting can provide other significant sources of error (e.g., size variations and non-uniform U and Th distributions in the dated grains, local fault offsets, local thermal anomalies, etc.). The residuals are normally distributed with a mean of 0.4 Ma and a standard deviation of 8 Ma. Our bootstrap analysis (reported below) is based on the residuals, so the estimated uncertainties for the parameters include all of the observed variance relative to the model fit.

However, another potential problem is error in the model itself, which could introduce bias in the results. For our case, the most likely model error is that isochronal surfaces have significant curvature over the scale of the study area. The spatial distribution of the residuals provides the best way to test if the model provides a reasonable

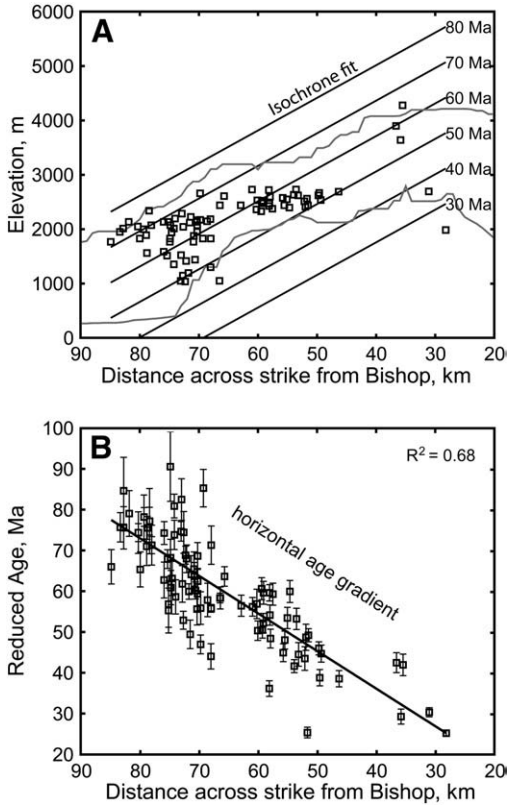

Fig. 3. The isochrone best-fit of bedrock cooling age data projected into down-dip cross section. A) The range of bedrock samples and best-fit isochrones are plotted relative to the maximum and minimum topography along the cross section. B) The quality of the isochrone fit is shown by reducing the observed ages according to the difference between each predicted age and predicted age at 2.2 km elevation. This is equivalent to plotting the model residuals around the mean. Error bars depict the 1-sigma analytical errors in the age measurements, and misfits outside these errors indicate error in the model fit. Recalculating the fit, omitting the Mt. Whitney vertical transect data (at 30 to 40 km), demonstrates that this does not significantly change the parameter results.

representation of the data. Fig. 2 shows the polarity of the residuals in map view. Fig. 3 shows the residuals in cross section. Neither figure shows evidence of spatially correlated residuals. We examine this issue in a more formal way using the Von Neumann Rank Ratio test (Bartels, 1982), which finds no significant spatial correlation (at the 5% level) in the residuals, for reduced-age plots along the principle axes of the mean topographic surface.

House et al. (1997) argued, based on along-strike transects, that apatite He cooling ages are inversely correlated with the modern topography of the southern Sierra Nevada. They inferred that this correlation meant that the topographic relief of this region at 80 to 30 Ma was similar to the relief observed today. Our analysis includes all of the data, rather than individual transects. If the House et al. (1997) interpretation is correct, then we should see a strong correlation between the residuals and the modern topography, but see no such correlation.

The best-fit solution, with all data included, indicates that the isochrones have an average strike of $151^\circ \pm 2^\circ$ and a westward dip of $3.4^\circ \pm 0.8^\circ$ (uncertainties are cited as 95% confidence intervals, as determined by the bootstrap method below). The strike is parallel to the range front, and the dip is steeper than the modern dip of the west flank of the range. Unruh (1991) reports a similar attitude for late Cenozoic strata in the northern Sierra.

Our best-fit model provides estimates of erosion rates at two different time intervals corresponding to the TF and AE methods (see Fig. 6 in Reiners and Brandon, 2006). We focus specifically on the erosion history of the centroid of the age data (Fig. 3), given that the parameter estimates are most representative of the history of that point. A more complete analysis would require consideration of the tilting, but our focus on the centroid allows us to ignore this issue. The centroid (Fig. 3) lies at an across-strike distance of 66 km and has a He apatite age of 60 Ma, as estimated by the best-fit for the tilted isochrones. The best-fit age gradient normal to the isochrones indicates that the centroid point has a vertical velocity of $0.06 \pm$ km/Ma relative to the effective closure isotherm. This is a version of the AE method. More limited "vertical transects" in the central and southern Sierra Nevada give similar rates of 0.05 km/Ma (House et al., 1997; House et al., 2001; Clark et al., 2005). This velocity is equivalent to the erosion rate at the centroid age, but only if the isotherm is in fact at steady state. The AE method can be biased by the influence of surface relief on the closure isotherm, but our tilt analysis spans a much larger area relative to a conventional AE analysis, so variations due to relief should be much reduced. The cooling age for the centroid point indicates the time-of-flight from the closure depth to its present location at the Earth's surface. The AGE2EDOT method (Reiners and Brandon, 2006) is used to derive from the cooling age a TF erosion rate, assuming a steady state 1D thermal profile with erosion included and given the closure properties of the He apatite system. This analysis gives a rate of 0.05 km/Ma, which represents the estimated steady erosion rate for the time 60 Ma to present. These estimates indicate that Sierra Nevada was eroded very slowly and in a remarkably steady manner throughout the Cenozoic. There may have been short-term variations but they were not of sufficient magnitude to show up in our long-term measurements. It is also important to note that the similarity of the rates for the two methods supports the steady state isotherm assumption, which underlies both the AE and TF methods.

5. Detrital cooling ages

5.1. Critical assumptions

Our tracer method relies on several key assumptions:

1. *Variations in erosion rate are uncorrelated with variations in the concentration of the tracer phase in the bedrock surface*. In general, one might worry about the effect of spatial variations in the concentrations of the dated mineral. The worst case would be if concentrations of the dated mineral were strongly correlated with the modern distribution of erosion rates. To the extent that granitic rocks of the Sierra Nevada have fairly homogeneous concentrations of apatite, this issue is not a major concern.
2. *The tracer phase is conserved during transport*. Wildfires have the potential to reset low-temperature thermochronometers, but Sierran apatite grains show little to no resetting by fire (Reiners et al., 2007). Alteration and dissolution of apatite by organic acids in soils may be a concern. As in the first assumption, the failure of this assumption only becomes important if the preservation of the detrital apatite is strongly correlated with the spatial distribution of erosion rates.
3. *The residence time of the tracer and the size of the drainage are both large enough to average out local variations in erosion processes both in time and space*. Unsteady processes, such as landslides, might cause this assumption to be violated. The mixing of stored and mobile sediment is an important buffer of unsteadiness. We note that this steadiness issue is also a concern for drainage-scale erosion rates estimated by cosmogenic ^{10}Be (Niemi et al., 2005). Both require the assumption that production of new sediment and removal of old sediment are in a quasi-steady state, when averaged over the residence times for the sediment moving through the drainage. For the ^{10}Be system, this requires that the production of ^{10}Be in the drainage is equal to the export of ^{10}Be. Although all drainages are affected by unsteady processes (such as landslides), experience in the ^{10}Be system indicates that the production-export assumption tends to work very well in large drainages and with long residence times because the sources of unsteadiness tend to be averaged out (Bierman and Nichols, 2004; Niemi et al., 2005).

5.2. Detrital-age distributions

The detrital CDFs are based on (U–Th)/He apatite grain ages from samples collected from sand bars in the lower reaches of the Kings and San Joaquin rivers in the foothills of the Sierra Nevada (Fig. 2). The samples were collected for a study of paleo-wildfires (Reiners et al., 2007). That work found only 2 grains which were reset by wildfire, and those are excluded here. Sample 04WFS14 from the San Joaquin River has 44 apatite grain ages, and sample 04WFS15 from the Kings has 50 apatite grain ages (see Reiners et al., 2007).

Each detrital-age distribution (Fig. 4) is significantly different (at the 5% level) from its bedrock-age distribution, as indicated by the Kolmogorov–Smirnov test. It is interesting that the detrital distribution for the Kings contains an excess of young ages relative to its bedrock distribution, whereas the San Joaquin contains a relative excess of older grains. The Kings and San Joaquin have similar patterns of bedrock ages, with young ages located in the valleys and old ages on the interfluves. The detrital-age distribution suggests that valley erosion is faster than interfluve erosion in the Kings, and that the opposite may be the case in the San Joaquin (although we need to assess the role of storage behind the dams in the San Joaquin before we can come to any specific conclusion). The relative density method, introduced next, provides a quantitative estimate of the pattern of relative erosion rates in these drainages.

6. Relative erosion rates and non-parametric kernel density estimation

6.1. Estimating relative densities

In terms of PDFs, the distribution of relative erosion rates, f_E, relates the distribution of mobile sediment to that of the upstream bedrock sources:

$$f_V(\tau) = f_E(F_A(\tau)) f_A(\tau). \quad (5)$$

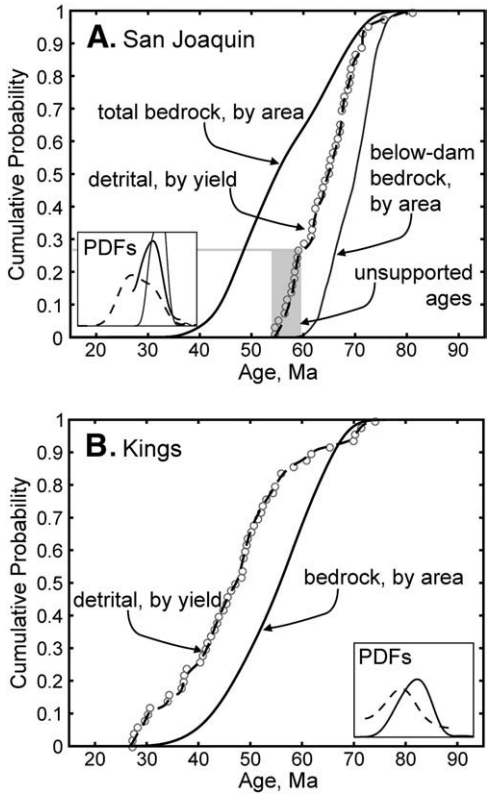

Fig. 4. Empirical cumulative probability plots for bedrock (solid) and detrital (dashed) cooling age data. The actual detrital data are plotted with circles. The plots simply depict the probability that a sample has a cooling age less than or equal to the given age. Equivalent probability density plots are inset. We use both cumulative probability and probability density in our analysis. Probability density plots require the estimation of a kernel width, which introduces an arbitrary degree of smoothing. Empirical cumulative probability plots provide a more transparent representation of the underlying age data. Therefore, we report age distributions with empirical cumulative probabilities, while we reserve density plots for relative erosion rate results, which by necessity incorporate some smoothing. A) The San Joaquin shows an abundance of old detrital ages relative to its bedrock distribution. Two bedrock distributions are given in the San Joaquin: the distribution for the total drainage area upstream of the detrital sample, and the distribution of the fraction of the drainage between the detrital sample and the first trunk stream dam. "Unsupported ages" are those detrital ages that cannot be derived from the below-dam bedrock-age distribution. B) The Kings shows an abundance of young detrital ages.

In statistics literature, f_E is called a relative density distribution, in that it represents the ratio of two probability density distributions (Handcock and Morris, 1999; Handcock and Janssen, 2002). For our analysis, f_E provides a comparison of the density of cooling ages by yield, $f_V(\tau)$, relative to the reference distribution, which is the density of cooling ages by area, $f_A(\tau)$, in the bedrock source region. A potential confusing aspect of this arrangement is that f_E is defined as a function of the cumulative probability, $P = F_A(\tau)$, for the ages by area. In this context, the probability should be viewed as a proxy for the range of cooling ages in the bedrock source region with $P = 0$ for the youngest age to $P = 1$ for the oldest.

We estimate f_E using the method of Handcock and Morris (1999, p. 140). The basic idea is to link the sampled cooling ages by yield to the cumulative probability distribution of the ages by area.

1) The first step is to estimate $F_A(\tau)$ using Eq. 3. $F_A(\tau)$ provides a one-to-one mapping between an observed age $T_{A,i}$ and the cumulative probability for that observed age $P_{A,i}$.
2) The next step is to use the measured detrital ages $T_{V,j}$ to generate an additional distribution of P_A values from $F_A(\tau)$. In essence, the detrital ages are being used to sample the cumulative distribution of bedrock ages. The sampled probabilities are given by $R_j = F_A(T_{V,j})$, where $j = 1$ to n grain ages in the detrital sample. These sampled values can then be used to generate an empirical cumulative probability distribution for the probability of the detrital ages by yield relative to the probability of the bedrock ages by area:

$$P_V = \hat{F}_R(P_A) = \frac{1}{n}\sum_{j=1}^{n} I\left(R_j \leq P_A\right). \quad (6)$$

3) The relative density distribution is simply the derivative of (6),

$$f_E(P_A) = \frac{d\hat{F}_R(P_A)}{dP_A}. \quad (7)$$

However, the empirical cumulative function $\hat{F}_R$ is not continuous, so it cannot be easily differentiated. The preferred approach is to estimate the probability density plot for f_E using the observed R_j values (Hanson and Morris, 1999). The PDF is best estimated using a non-parametric kernel density estimator (Rosenblatt, 1956; Silverman, 1986). Our preferred density estimator is based on the work of Jones et al. (1995) and Botev (2007). Botev (2007) presents an automatic method for estimating the optimal size of the kernel, which ensures that the compromise among precision, resolution, and smoothness minimizes the asymptotic mean squared error of the estimate. We have added to his algorithm (kde.m, available at www.mathworks.com/matlabcentral) the method of Jones et al. (1995), which reduces the bias that results from the smoothing necessary for density estimation. The modified Matlab program is called kdeJNL.m (see Supplementary materials) and provides the best available method for density estimation at this time.

The relative density results (Fig. 5) are consistent with our expectations from the bedrock and detrital CDFs. The distributions of erosion rates differ greatly in the two drainages. In the San Joaquin, peak erosion rates occur where surface bedrock ages are ~85 Ma, whereas those in the Kings drainage occur where surface bedrock ages are younger, ~35 Ma. These maxima are eroding ~3 times faster than the drainage means, while minimum rates approach zero in both drainages.

6.2. Spatial variation of erosion rates and relief change

Fig. 6 shows map views of relative erosion rates. These are generated by mapping the relative densities onto the DEM, with the bedrock ages providing the common variable. The Kings map shows the fastest erosion in the valleys and the slowest erosion on the interfluves. In contrast, the San Joaquin map shows that erosion is fastest on the interfluves and slowest in the deeper valleys. These results suggest that relief is presently increasing in the Kings drainage, and possibly decreasing in the San Joaquin (depending on the issue of dam storage). One caveat about these maps is that the bedrock ages provide only a crude linkage between erosion rates and cooling ages. As an example, we noted above that erosion is about 3 times faster than average in the Kings drainage where bedrock ages are about 35 Ma. This estimate represents an average for the entire area where 35 Ma bedrock is exposed. It provides no information about variations in erosion rates within this area. The Kings and San Joaquin drainages do not seem to be significantly influenced by this issue given that the river channels and interfluves lie at a high angle to the contours of bedrock cooling ages. Our first assumption – that erosion rates should be largely uncorrelated with bedrock cooling ages – seems to work for these drainages.

The bootstrap method (Efron and Tibshirani, 1986) provides an ideal way to assess our results. In particular, it provides a way to assess how our final estimates are influenced by all sources of random error. The key idea is to use random sampling to generate replicate data sets and to evaluate the variation in the estimated results associated with

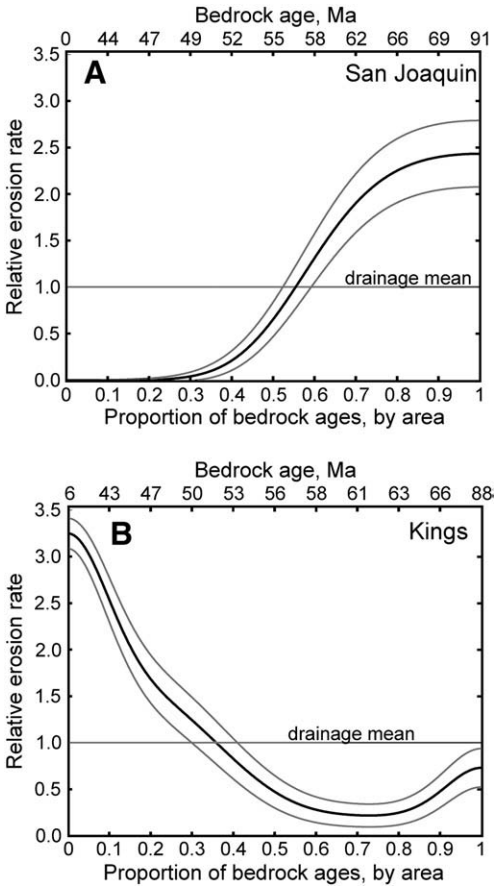

Fig. 5. Erosion rates as relative density distributions for A) the San Joaquin River drainage and B) the Kings River drainage. The San Joaquin has the fastest erosion rates where bedrock ages are oldest. In contrast, the bedrock surfaces with the youngest ages are eroding fastest in the Kings. Note that the mean erosion rates are not the same, in absolute terms, in both drainages. Error envelopes refer only to error in the density estimate (see Supplementary materials).

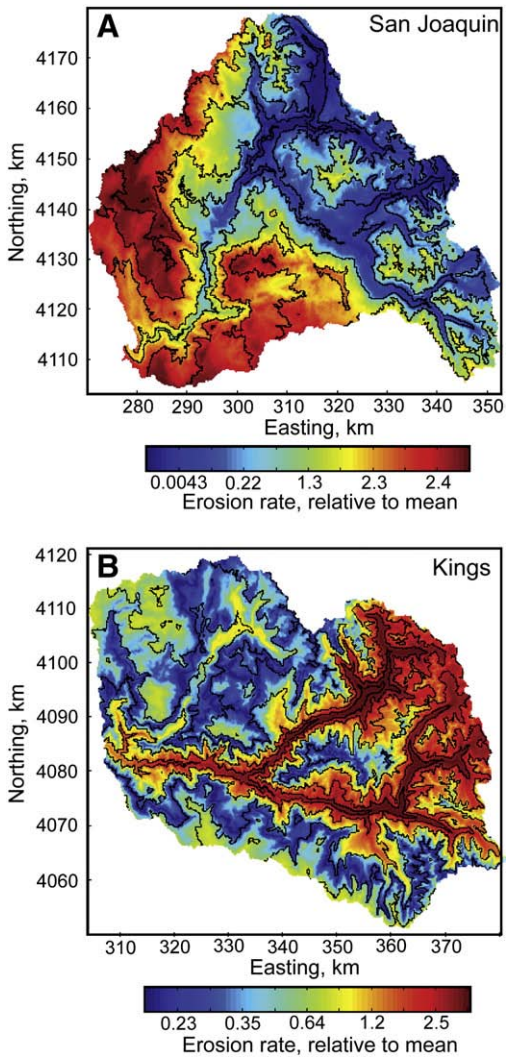

Fig. 6. Maps of relative erosion rates in A) the San Joaquin River drainage and B) the Kings River drainage. Topography is contoured in black, while relative erosion rates are colored. Note that erosion rates in the drainages are relative to different mean values. Fastest erosion occurs on the interfluves of the San Joaquin but in the channels of the Kings. In both drainages, the particular correlation of relief and erosion rates indicates relief change.

the replicates. Our bootstrap analysis is based on the generation and analysis of 1000 replicate datasets for each drainage. Each replicate detrital-age dataset is generated by selecting at random and with replacement from the original detrital-age dataset. This replicate dataset has the same number of grain ages as the original but is otherwise different given the random sampling. A replicate set of bedrock ages is determined by using the bedrock ages predicted by the best-fit model and adding a random sampling with replacement of the residuals to these predicted ages. These replicate data are analyzed in the same way as the original data. The resulting 1000 replicate estimates show how the variation in the data propagates through the analysis as indicated by the distributions of replicates for each of the parameter estimates (Carpenter and Bithell, 2000). The confidence intervals reported in this paper are determined by finding the 95% limits from the distribution of the replicate estimates.

We are interested in evaluating the polarity of relief change, which is related to how erosion rates correlate with modern relief. It is useful to define the local relief as the height of a point relative to the mean surface of the landscape, as determined by fitting a planar surface to the topography of the drainage. The best-fit plane for the topography of the Kings and San Joaquin drainages has a strike of 155° and a dip of 1.9° west. A negative correlation between the local erosion rate and local relief would indicate that the overall relief of the drainage was increasing given that valleys were eroding faster than interfluves. A positive correlation would indicate the opposite situation, where the overall relief is decreasing with time. The two left panels in Fig. 7(A and C) show how local relief and local erosion rate vary for all of the DEM pixels for the best-fit solutions for the San Joaquin and Kings drainages. The dashed lines are determined by linear regression and provide a simple representation of the overall trend of local erosion rates as a function of local relief. As expected, the data show positive and negative trends for the San Joaquin and Kings, respectively.

The bootstrap replicates are particularly useful for evaluating these trends. The right panels (Fig. 7B and D) show the results of 1000 replicate calculations. The contours show the density distribution for point values generated for all of the bootstrap replicates. The dashed "bowtie" region in each panel shows the 95% confidence range of the slopes of the best-fit trend lines calculated for each of the 1000 bootstrap replicates. These results clearly show that the contrasting trends for the Kings and San Joaquin are well defined by the data. The evidence seems quite clear that the overall relief of the Kings is presently increasing with time. The opposite appears true for the San Joaquin, but the influence of the many dams must be assessed before reaching a conclusion.

6.3. Dams and sediment storage

Sediment storage is a common feature of all drainages. Natural examples include fill deposits and bars, which tend to form

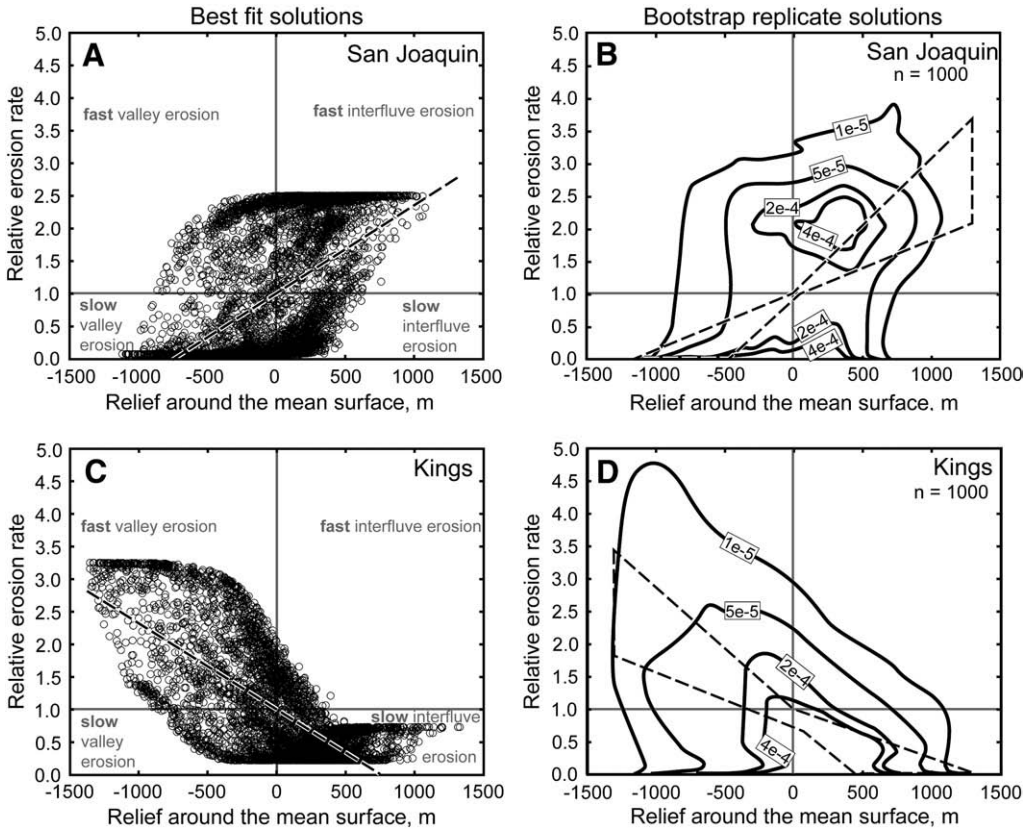

Fig. 7. Bootstrap error analysis of relief change in the Sierra Nevada, where relief is distance from a dipping, mean elevation plane oriented 155°/1.9°. A positive correlation indicates decreasing relief while a negative correlation indicates increasing relief. A) Best fit results for relative erosion rates on the DEM in the San Joaquin, indicating relief decay. The linear regression (dashed) is plotted to guide the eye. B) Monte Carlo results for 1000 complete replicate calculations in the San Joaquin, also showing a positive trend and decaying relief. Contours depict the density of points. The range of linear regression for the central 95% of replicates is plotted to guide the eye. C) Best fit results in the Kings. D) Bootstrap results in the Kings, also using 1000 complete replicates.

episodically along active bedrock rivers, and lacustrine sediments, which accumulate behind dammed segments of a river. Stranded glacial deposits and colluviated hollows are other natural examples of storage. Although storage is almost always ephemeral, the duration may be long, on the order of 100 to 10 ka, as indicated by our assessment of residence times above. Man-made dams are an extreme form of sediment storage. Dams generally capture the entire upstream sediment load carried by the river, but this capture typically lasts less than 50 to 75 years. We focus here on the sediment storage behind dams in the San Joaquin drainage because the dense network of dams there should provide an end-member example.

Despite the prevalence of dams in the San Joaquin, there is clear evidence that a large fraction of the detrital sediment sample was derived from upstream of the lowest dam. This dam, at Redinger Lake, is located just 11 km upstream from the detrital sampling point (Fig. 2). Fig. 4a shows the bedrock-age distribution for this small part (10%) of the drainage as well as the detrital-age distribution. The downstream bedrock has no ages younger than 58 Ma, and yet about 25% of the detrital-age distribution is younger than this. These younger ages require an upstream source because they are unsupported by downstream bedrock ages. We interrogate the bootstrap results to infer the probability that error in the bedrock model fit could cause this discrepancy. We find that there is only an 11% probability that the downstream bedrock could support all of the detrital ages by chance alone.

The reservoirs on the San Joaquin are drained by pipes or rock tunnels that lie close to the deepest parts of the reservoirs, so it is possible that some sand is able to circumvent the dams, but the amount is probably small. A more likely possibility is that our detrital sample includes sediment that was mobilized from the alluvial deposits along the river below Redinger Lake. Several fill terraces are visible in aerial photography for this lower reach. These fills likely store well-mixed sediment that was transported from the upper reaches of the drainage prior to dam construction (Janda, 1966). An under-capacity river, such as one exiting a dam, tends to gradually return to full sediment transport capacity by laterally eroding its banks. The river may also vertically incise, but this would be a slower process in the largely bedrock channel. Although the volume of the visible fills is small, the sediment loads of the San Joaquin are also small enough (Anderson, 1974) that remobilized sediment could reasonably constitute a large fraction of the total load.

Given evidence of sediment mixing, we explore the effect of various proportions of upstream and downstream mixing on our relative erosion rate measurement. We rewrite Eq. 5 in terms of the linear combination of the upper and lower bedrock-age distributions, f_{Au} and f_{Ad}, respectively:

$$f_V = \alpha f_E f_{Au} + (1-\alpha) f_E f_{Ad}. \quad (8)$$

The parameter α represents the fraction of the total detrital-age distribution derived from the drainage area above the Redinger Lake Dam. In order to account for the fraction of detrital grains younger than 58 Ma, α must be larger than 25%. Fig. 8 shows the result of the relative erosion rate calculation using Eq. 8 with $\alpha = 25\%$, which suggests stagnating relief in the San Joaquin. This is a conservative result because 25% is a minimum value, and the result will approach

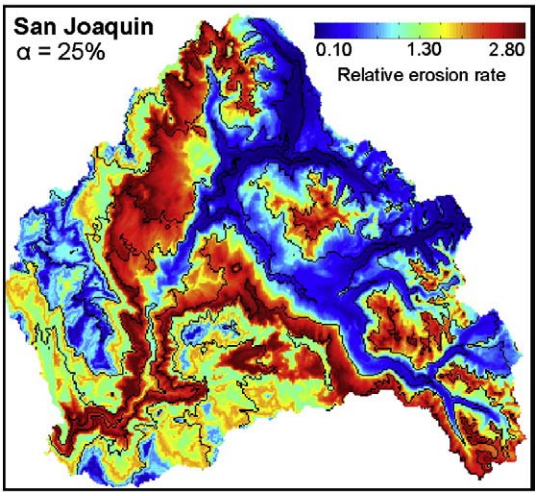

Fig. 8. Possible effect of sediment trapping behind dams on the San Joaquin erosion rate calculation. Using linear mixing model (see text), we perform the tracer analysis assuming that only 25% of the detrital sample is derived from upstream of the Redinger Lake Dam, which is the minimum fraction required by the CDFs. As the fraction approaches 90%, the fraction of area above the dam, the plot will approach the result in Fig. 6A.

the result in Fig. 6A as α approaches 90%. We note that stagnating or decaying relief is also consistent with the absence in the detrital-age distribution of the 50 to 30 Ma ages that are abundant in the total bedrock-age distribution (Fig. 4A). However, Eq. 8 requires the assumption of a single erosion rate distribution – of arbitrary shape – in both the upstream and downstream areas, which is impossible to verify without addition detrital sampling. Therefore, we have only a weak preference for stagnating or decaying relief in the San Joaquin. The most robust result of the tracer analysis in the San Joaquin is that the storage and remobilization of sediment is a buffer that tends to average out the effects of unsteady processes, likely including man-made dams.

7. Discussion

7.1. Isochrone deformation and long-term erosion rates

Dipping isochrones in the Kings and San Joaquin drainages are direct evidence that tilting occurred at least as far south as the latitude of Mt. Whitney. The range of isochrone ages involved in tilting indicates that deformation began after ~35 Ma, the age of the youngest bedrock cooling ages. Because the isochrones also fit to bedrock dates farther north, they indicate that this pattern was coincident with tilting in there as well. The timing and magnitude of tilting are consistent with geologic evidence in the north for a few degrees of westward tilting at ~5 Ma (e.g., Unruh, 1991; Wakabayashi and Sawyer, 2001). The 3.4° isochrone dip is consistent with gentle westward dips in the Great Valley strata, which onlaps the western edge of the Sierra Nevada, although the dips in the Great Valley strata are typically around 1.4°.

The isochrone fit across Sierra Nevada also indicates that the erosion rate during the Cenozoic was slow and steady. Major departures from the 0.06 km/Ma rate would have created variations in the isochrone gradient, distorting the model fit. This AE-type erosion rate provides regional-scale measurement, and the effect of any paleorelief on the form of the isochrones is small compared to the regional tilting. The TF results support the long-term erosion rate of 0.05 to 0.06 km/Ma. Recent, short-duration incision events (e.g., Stock et al., 2005) are not resolved by this method.

7.2. Relief change and implications for lower lithosphere removal

A likely explanation for relief growth in the Kings drainage is the loss of part of the underlying lithosphere. In fluvial settings like the Sierra Nevada, relief is sensitive to topographic gradients (e.g., Howard, 1994). Numerical experiments predict initial subsidence above an unstable lithospheric root as it starts to detach, followed by uplift after it has drops through the sublithospheric mantle (Le Pourhiet et al., 2006; Gogus and Pysklywec, 2008). Seismic and petrographic evidence suggest complete root detachment below the Kings drainage peaks, which would result in uplift of the eastern side of the range (Wernicke et al., 1996; Ducea and Saleeby, 1996; Ducea and Saleeby, 1998; Boyd et al., 2004; Yang and Forsyth, 2006). The Isabella velocity anomaly, observed ~150 km beneath the eastern Great Valley and the foothills of the Southern Sierra Nevada, is thought to represent part or all of the foundered lithospheric root (Ruppert et al., 1998; Zandt et al., 2004). Quaternary subsidence of the Tulare Dry Lake Bed above the Isabella anomaly can be explained by westward drift of the detached root and the viscous load that it causes as it settles through the mantle (Saleeby and Foster, 2004; Gilbert et al., 2007). These interpretations would predict an increase in incision rates in the Kings drainage because of the increase in topographic gradients across the west side of the Sierra Nevada. Local responses to deep lithospheric processes are reasonable in the Sierra Nevada, where the elastic thickness of the crust is very small (Granger and Stock, 2004).

Our results for the San Joaquin drainage are less definitive. Nonetheless, the evidence suggests that relief there is either steady or decaying. If correct, then it would seem that the San Joaquin lies north of the region thinned by the detachment of the lithospheric root. There are few other possible causes of the contrast in relief change, given that the San Joaquin and Kings drainages share common precipitation, glacial history, and bedrock lithology (e.g., Reibe et al., 2001).

8. Conclusions

The application of tracer thermochronology to the Sierra Nevada shows relief creation in the Kings River drainages in the last 100 to 10 ka. In contrast, relief is probably stagnant or decaying in the San Joaquin. Dams and other kinds of storage limit this method, but the impact may not be as extreme as expected. We suggest that a foundering lithospheric root is the best explanation for relief change in the southern Sierra Nevada. The contrasting states of relief change in the Kings and the San Joaquin drainages suggest that the loss of lower lithospheric root is presently limited to the Kings River drainage and south. This is permissible given available data, and awaits confirmation by additional seismic results.

At longer timescales, our analysis suggests that much of the Sierra Nevada shares a common history of deformation and exhumation. Isochrones, extending well north and south of the drainages in question, were tilted 3.4° to the southeast sometime after ~35 Ma. Isochrone deformation is consistent with other geologic evidence for tilting at ~5 Ma, independent of the loss of the root. Exhumation rates measured with both the isochrone gradient (AE) and TF methods are 0.05 to 0.06 km/Ma, suggesting that exhumation was largely steady through the history of the Sierra Nevada, at least until a period of range-wide incision from ~5 to 3 Ma, which was followed by much lower rates.

The tracer thermochronology method presented here measures relative erosion rates at a scale sufficient to distinguish differences between ridges and valleys, or among other large landforms in river drainages. All tracer methods are based on linking a volume of detrital sediment to upstream sources, generally using cooling ages as the link. We present two innovations that establish a foundation for tracer thermochronology. First, we introduce isochrones, or surfaces of equal

cooling age. By treating these surfaces as a form of stratigraphy, we map predicted bedrock ages and learn about the long-term history of deformation and exhumation. Second, we estimate relative erosion rates over the surfaces of the drainages. Non-parametric kernel density estimation with an ideal-width kernel makes these estimates with minimal assumptions and the smallest possible error. The technique is demonstrated to be robust in the Sierra, where it provides previously unavailable insight into landscape change.

Acknowledgements

We thank Rebecca Flowers, Peter Van Der Beek and two anonymous reviewers for detailed, critical reviews and T. Mark Harrison for editorial oversight. This feedback helped reveal some important shortcomings in our analysis and interpretations, especially regarding the influence of man-made dams.

Appendix A. Supplementary data

Supplementary data associated with this article can be found, in the online version, at doi:10.1016/j.epsl.2010.05.022.

References

Anderson, H.W., 1974. Sediment deposition in reservoirs associated with rural roads, forest fires, and catchment attribute. Proceedings of the Symposium on Man's Effect on Erosion and Sedimentation. : Publication, 113. International Association of Hydrological Sciences, Wallingford, England, pp. 87–95.
Bartels, R., 1982. The rank version of the Von Neumann ratio test for randomness. J. Am. Stat. Assoc. 77, 40–46.
Bates, R.L., Jackson, J.A., 1987. Glossary of Geology, 3rd edition. American Geological Institute, Alexandria, VA. pp. 754.
Bernet, M., Brandon, M.T., Garver, J.I., Balestieri, M.L., Ventura, B., Zattin, M., 2009. Exhuming the Alps through time: clues from detrital zircon fission track thermochronology. Basin Res. doi:10.1111/j.1365-2117.2009.00400.x.
Bierman, P., Nichols, K.K., 2004. Rock to sediment – slope to sea with ^{10}Be – rates of landscape change. Annu. Rev. Earth Pl. Sc. 32, 215–255.
Botev, Z.I., 2007. Nonparametric Density Estimation via Diffusion Mixing. URL: http://www.maths.uq.edu.au/~botev/.
Boyd, O.S., Jones, C.H., Sheehan, A.F., 2004. Foundering lithosphere imaged beneath the Southern Sierra Nevada, California, USA. Science 305, 660–662.
Brewer, I.D., Burbank, D.W., Hodges, K.V., 2003. Modelling detrital cooling-age populations: insights from two Himalayan catchments. Basin Res. 15, 305–320.
Braun, J., 2003. Pecube: a new finite-element code to solve the 3D heat transport equation including the effects of a time-varying, finite amplitude surface topography. Comput. Geosci. 29, 787–794.
Braun, J., 2002. Quantifying the effect of recent relief changes on age-elevation relationships. Earth Planet. Sci. Lett. 200, 331–343.
Carpenter, J., Bithell, J., 2000. Bootstrap confidence intervals: when, which, what? A practical guide for medical statisticians. Stat. Med. 19, 1141–1164.
Chase, C.G., Wallace, T.C., 1988. Flexural isostasy and uplift of the Sierra Nevada of California. J. Geophys. Res. 93, 2795–2802.
Clark, M.K., Gweltaz, M., Saleeby, J., Farley, K.A., 2005. The non-equilibrium landscape of the southern Sierra Nevada, California. GSA Today 15, 4–10.
Dixon, T.H., Miller, M., Farina, F., Wang, H., Johnson, D., 2000. Present-day motion of the Sierra Nevada block and some tectonic implications for the Basin and Range province, North America Cordillera. Tectonics 19, 1–24.
Dodson, M.H., 1973. Closure temperature in cooling geochronological and petrological systems. Contrib. Mineral. Petrol. 40, 259–274.
Ducea, M.N., Saleeby, J.B., 1996. Buoyancy sources for a large, unrooted mountain range, the Sierra Nevada, California: evidence from xenolith thermobarometry. J. Geophys. Res. Sol. Ea. 101, 8229–8244.
Ducea, M.N., Saleeby, J.B., 1998. The age and origin of a thick mafic–ultramafic keel from beneath the Sierra Nevada batholith. Contrib. Mineral Petr. 133, 169–185.
Dumitru, T.A., 1990. Subnormal geothermal gradients in the extinct Sierra Nevada magmatic arc: consequences of Laramide and post-Laramide shallow-angle subduction. J. Geophys. Res. 95, 4925–4941.
Efron, B., Tibshirani, R.J., 1986. Bootstrap methods for standard errors, confidence intervals, and other measure of statistical accuracy. Stat. Sci. 1, 54–77.
Farmer, G.L., Glazner, A.F., Manley, C.R., 2002. Did lithospheric delamination trigger late Cenozoic potassic volcanism in the southern Sierra Nevada, California? GSA Bulletin 114, 754–768.
Gayer, E., Mukhopadhyay, S., Meade, B.J., 2008. Spatial variability of erosion rates inferred from the frequency distribution of cosmogenic ^{3}He in olivines from Hawaiian river sediments. Earth Planet. Sci. Lett. 266, 303–315.
Garver, J.I., Brandon, M.T., 1994. Erosional denudation of the British Columbia Coast Ranges as determined from fission-track ages of detrital zircon from the Tofino basin, Olympic Peninsula, Washington. Geol. Soc. Am. Bull. 106, 1398–1412.
Gilbert, H., Jones, C., Owens, T.J., Zandt, G., 2007. Imaging the Sierra Nevada lithospheric sinking. Eos 88, 225–229.
Gogus, O.H., Pysklywec, R.N., 2008. Near-surface diagnostics of dripping or delaminating lithosphere. J. Geophys. Res. 113. doi:10.1029/2007JB005123.
Granger, D.E., Stock, G.M., 2004. Using cave deposits as geologic tiltmeters: application to postglacial rebound of the Sierra Nevada, California. Geophys. Res. Lett. 31. doi:10.1029/2004GL021403.
Handcock, M.S., Morris, M., 1999. Relative Distribution Methods in the Social Sciences. Springer-Verlag, New York. 265 p.
Handcock, M.S., Janssen, P.L., 2002. Statistical inference for relative density. Sociol. Method. & Res. 30, 394–424.
House, M.A., Wernicke, B.P., Farley, K.A., Dimitru, T.A., 1997. Cenozoic thermal evolution of the central Sierra Nevada, California, from (U–Th)/He thermochronometry. Earth Planet. Sc. Lett. 151, 167–179.
House, M.A., Wernicke, B.P., Farley, K.A., 1998. Dating topography of the Sierra Nevada, California, using apatite (U–Th)/He ages. Nature 396, 66–69.
House, M.A., Wernicke, B.P., Farley, K.A., 2001. Paleo-geomorphology of the Sierra Nevada, California, from (U–Th)/He ages in apatite. Am. J. Sci. 301, 77–102.
Howard, A.D., 1994. A detachment-limited model of drainage basin evolution. Water Resour. Res. 30, 2261–2285.
Janda, R. J., 1966. Pleistocene history and hydrology of the upper San Joaquin River, California. Ph.D. thesis. University of California, Berkeley.
Jones, M.C., Linton, O., Nielson, J.P., 1995. A simple bias reduction method for density estimation. Biometrika 82, 327–338.
Le Pourhiet, L., Gurnis, M., Saleeby, J., 2006. Mantle instability beneath the Sierra Nevada Mountains in California and Death Valley extension. Earth Planet. Sc. Lett. 251, 104–119.
Linn, A.M., DePaolo, D.J., Ingersoll, R.V., 1992. Nd–Sr isotopic, geochemical, and petrographic stratigraphy and paleotectonic analysis: Mesozoic Great Valley forearc sedimentary rocks of California. Geol. Soc. Am. Bull. 104, 1264–1279.
Maheo, G., Saleeby, J., Saleeby, Z., Farley, K.A., 2009. Tectonic control on the southern Sierra Nevada topography, California. Tectonics 28. doi:10.1029/2008TC002340.
Mancktelow, N.S., Grasemann, B., 1997. Time-dependent effects of heat advection and topography on cooling histories during erosion. Tectonophysics 270, 167–195.
Menke, G., 1984. Geophysical data analysis: discrete inverse theory. : International Geophysics Series, 45. Elsevier, San Diego, CA. 289 pp.
Molnar, P., England, P., 1990. Late Cenozoic uplift of mountain ranges and global climate change: chicken or egg? Nature 346, 29–34.
Niemi, N.A., Oskin, M., Burbank, D.W., Heimsath, A.M., Gabet, E.J., 2005. Effects of bedrock landslides on cosmogenically determined erosion rates. Earth Planet. Sc. Lett. 237, 480–498.
Reibe, C.S., Kirchner, J.W., Granger, D.E., Finkel, R.C., 2001. Minimal climatic control on erosion rates in the Sierra Nevada, California. Geology 29, 447–450.
Reiners, P.W., Thomson, S.N., McPhillips, D., Donelick, R.A., Roering, J.J., 2007. Wildfire thermochronology and the fate and transport of apatite in hillslope and fluvial environments. J. Geophys. Res. Earth 112. doi:10.1029/2007jf000759.
Reiners, P.W., Brandon, M.T., 2006. Using thermochronology to understand orogenic evolution. Annu. Rev. Earth. Pl. Sc. 34, 419–466.
Rosenblatt, M., 1956. Remarks on some nonparametric estimates of a density function. Ann. Math. Statist. 27, 832–837.
Ruhl, K.W., Hodges, K.V., 2005. The use of detrital mineral cooling ages to evaluate steady state assumptions in active orogens: an example from the central Nepalese Himalaya. Tectonics 24. doi:10.1029/2004TC001712.
Ruppert, S., Fliedner, M.M., Zandt, G., 1998. Thin crust and active upper mantle beneath the southern Sierra Nevada in the western United States. Tectonophysics 286, 237–252.
Saleeby, J., Foster, Z., 2004. Topographic response to mantle lithosphere removal in the southern Sierra Nevada region, California. Geology 32, 245–248.
Saleeby, J., Saleeby, Z., Nadin, E., Maheo, G., 2009. Step-over in the Structure controlling the regional west tilt of the Sierra Nevada microplate: eastern escarpment system to Kern Canyon system. Int. Geol. Rev. 51, 634–669.
Silverman, B.W., 1986. Density Estimation for Statistics and Data Analysis. Chapman and Hall. 175 pp.
Small, E.E., Anderson, R.S., 1995. Geomorphically driven Late Cenozoic uplift in the Sierra Nevada, California. Science 270, 277–280.
Stock, G.M., Anderson, R.S., Finkel, R.C., 2004. Pace of landscape evolution in the Sierra Nevada, California, revealed by cosmogenic dating of cave sediments. Geology 32, 193–196.
Stock, G.M., Anderson, R.S., Finkel, R.C., 2005. Rates of erosion and topographic evolution of the Sierra Nevada, California, inferred from cosmogenic Al-26 and Be-10 concentrations. Earth Surf. Proc. Land. 30, 985–1006.
Stock, G.M., Ehlers, T.A., Farley, K.A., 2006. Where does sediment come from? Quantifying catchment erosion with detrital apatite (U–Th)/He thermochronometry. Geology 34, 725–728.
Stock, J.D., Montgomery, D.R., 1996. Estimating palaeorelief from detrital mineral age ranges. Basin Res. 8, 317–327.
Unruh, J.R., 1991. The uplift of the Sierra Nevada and implications for late Cenozoic epeirogeny in the western Cordillera. Geol. Soc. Am. Bull. 103, 1395–1404.
Vermeesch, P., 2007. Quantitative geomorphology of the White Mountains (California), using detrital apatite fission track thermochronology. J. Geophys. Res. 112, 3004.
Wagner, G.A., Reimer, G.M., 1972. Fission track tectonics: the tectonic interpretation of fission track ages. Earth Planet. Sci. Lett. 14, 263–268.
Wahrhaftig, C., Birman, J.H., 1965. The Quaternary of the Pacific mountain system in California. In: Wright, H.E., Frey, D.G. (Eds.), The Quaternary of the United States. Princeton University Press, pp. 299–340.

Wakabayashi, J., Sawyer, T.L., 2001. Stream incision, tectonics, uplift and evolution of topography of the Sierra Nevada, California. J. Geol. 109, 539–562.

Wernicke, B., Clayton, R., Ducea, M., Jones, C.H., Park, S., Ruppert, S., Saleeby, J., Snow, J.K., Squires, L., Fliedner, M., Jiracek, G., Keller, R., Klemperer, S., Luetgert, J., Malin, P., Miller, K., Mooney, W., Oliver, H., Phinney, R., 1996. Origin of high mountains in the continents: the southern Sierra Nevada. Science 271, 190–193.

Yang, Y., Forsyth, D.W., 2006. Rayleigh wave phase velocities, small-scale convection, and azimuthal anisotropy beneath southern California. J. Geophys. Res. 111. doi:10.1029/2005JB004180.

Zandt, G., Gilbert, H., Owens, T.J., Ducea, M., Saleeby, J., Jones, C.H., 2004. Active foundering of a continental arc root beneath the southern Sierra Nevada in California. Nature 431, 41–46.